






Article

Decentralized Control for the Cell Power Balancing of a Cascaded Full-Bridge Multilevel Converter

Miguel Vivert ¹ , Rafael Diez ² , Marc Cousineau ^{3*} , Diego Bernal Cobaleda, ⁴  and Diego Patino ² 

- ¹ Carrera de Ingeniería en Electricidad (CIELE), Facultad de Ingeniería en Ciencias Aplicada (FICA), Universidad Técnica del Norte, Ibarra, 100105, Ecuador; mevivert@utn.edu.ec (M.V.)
- ² Department of Electronics Engineering, Pontificia Universidad Javeriana, Bogotá ,110231, Colombia; rdiez@javeriana.edu.co (R. D.), patino-d@javeriana.edu.co (D. P.)
- ³ LAPLACE, Université de Toulouse, CNRS, INPT, UPS, 31071, Toulouse, France; marc.cousineau@laplace.univ-tlse.fr (M. C.)
- ⁴ Electrical Engineering Department (ESAT) KU Leuven - EnergyVille Diepenbeek -Genk, 3001, Belgium; diego.bernal@kuleuven.be (D. B. C.)
- * Correspondence: marc.cousineau@laplace.univ-tlse.fr; Tel.: +33-764-49-54-65 (M. C.)

Abstract: In modern inverter applications, multilevel converters are used thanks to their capability of reducing the passive filter volumes, improving the overall THD, sharing the power sources across the several converter cells, and providing a reconfiguration ability in case of failure. However, increasing the number of cells makes more complex the control of the converter. This article proposes a decentralized control technique based on the use of elementary modular controllers, associated with each converter cell and communicating with their close neighbors to obtain the balancing of the powers they supplied. Each modular controller can be dynamically removed or added to allow reconfiguration of the converter for functional safety purpose. This method is applied to a 240V/3A 5-cells Cascaded Full-Bridge Multilevel Converter. The response of the system to load transients and cell voltage disturbances demonstrates the robustness of the proposed decentralized control method. Thanks to the use of modular controllers, the number of levels of the converter can be extended to the order N without adding complexity to its control.

Keywords: Multilevel Converter; Cascaded Multilevel Converter; Decentralized control; Dis-tributed control, Balancing Controller; Converter Reconfiguration; Fault tolerant controller

1. Introduction

In the last decades, power electronics have been used in several applications, such as energy conversion and transmission, electrical traction, and storage systems. In all of these cases, the power converters have a key role, converting the energy of the source into a suitable one for the load, which are based on passive elements and switching devices such as MOSFETs or IGBTs [1,2]. For low and medium-voltage applications, MOSFETs and IGBTs are relatively fast and offer the advantage of controlling device turns on and off. However, these switching devices are limited for high power/voltage applications due to their voltage and current maximum value or switching time.

One solution for high power/voltage management is using Multi-Cellular Converters (MCC). The idea of MCCs is to “divide and rule”. These converters consist of an arrangement of several cells connected in parallel, in series, or in cascade, allowing the voltage or current distribution at the input or the output. There are many types of MCCs, such as the Flying Capacitor Multilevel Converter (FCMC) [3–7], where the input voltage is distributed among the cell voltages; Cascaded Full Bridge Multilevel Converter (CFBMC) [8–13], where the total output voltage is the sum of the output voltage of each Full Bridge (FB); and Multiphase Buck Converter, where its output current is the sum of the leg current [14–16]. In all these cases the energy is distributed among the cells, allowing the use of

low or medium-power devices for high-power applications. This fact is a great advantage because, normally, low-power devices are faster and more efficient than high-power ones. Therefore, MCCs allow managing high power conversion with low power and fast switching devices. Another feature of the multi-cellular converters is that with suitable frequency modulation techniques [17–20] it is possible to obtain a much higher output frequency than the MOSFETs or IGBTs switching frequency.

MCCs offer many advantages, however, there are a lot of challenges to be solved for these topologies. One of them is the ability to balance one variable of the cells according to the application. In FCMC, it is very useful that the capacitor voltages are balanced. Well-balanced capacitor voltages produce the supplied power distributed equally in all the cells. Furthermore, it makes a suitable ripple output voltage [3,4,21]. In the case of Multiphase Buck, balancing the leg current produces an appropriate distribution of the output current of the system [16]. For the case of CFBMC, it is possible to balance the output voltages of each FB to maintain equalized the power delivered by each FB [22–25]. For the same converter, if the sources are batteries, balancing the input current of each FB maintaining well-balanced the charging or discharging of the batteries, making also possible to control their State Of Charge (SOC). All these cell-variables balancing strategies can turn very complicated if the number of cells increases significantly.

Another challenge for Multi-cellular converters is the ability to insert or remove cells during operation [3,15,21,23], allowing to increase the power of the converter or giving a fault tolerance ability.

There exist many controllers that satisfy all these specifications. In [3,21], a control structure is proposed applied for an FCMC, which balances the capacitor voltages, regulates the output current, and allows a cell insertion/removal ability, obtaining interesting results.

The present work applies in the CFBMC the controller proposed in [3,21], develops a mathematical approach of the controller used in this topology, and shows the simulation and experimental results.

Section two describes the topology of the CFBMC and models it. The next section presents a description of the decentralized controller. Then in the fourth section, an in-depth analysis of the controller applied to the CFBMC is shown, presenting the closed-loop and open-loop transfer function and analyzing the bandwidth of the system. In section five, the design of the controller is presented, based on the open loop transfer functions of the system, obtaining, theoretically, the eigenvalues of the system. Then, section six presents the simulation and experimental results with three tests: load step, input voltage step, and cell insertion tests. Finally, the conclusion and future works are presented in the seventh section.

2. Description of the system

This article proposes an adaptation of a decentralized control applied previously to FCMC in [3,21], now implemented in a CFBMC of N Full-Bridges with inductive filter and resistive load. Fig. 1 shows the topology of the converter, using MOSFET as the switching device, where the control is implemented, where S_{yk} , represents the position of the high-side switches, 1, if it is in ON state, and 0 if it is in OFF state, for the k^{th} Full-Bridge (FB), $k = 1, 2, \dots, N$, $y = a$ for the left side branch of the k^{th} Full-Bridge and $y = b$ for the right side. $\overline{S_{yk}}$ is the complementary signal of S_{yk} . v_{ek} , v_{Hk}^{sw} , v_{Ck}^{sw} , i_k^{sw} are: the input voltage, the switching output voltage, the switching FB cell input capacitor voltage and the switching FB cell input inductance current of the k^{th} FB, respectively, while i_o^{sw} and v_o^{sw} correspond to the output current and voltage of the inverter, respectively. Depending on the position of the switches, the value of S_{yk} varies and also the internal cell signals. In order to simplify the equations, a slow variation assumption is made, compared to the switching frequency and an average model can be proposed, where the variable x is the moving average of the x^{sw} , and x can be: v_{Hk} , v_{Ck} , i_k , v_o i_o . In this work, the goal is to balance the moving average of the output voltage of the Full-Bridges, v_{Hk} , called the Cell Voltage (CV) and to regulate the output current, i_o , which is the Global Variable (GV) and

to provide a means of easily inserting or removing an FB cell without adding complexity to the balancing control system.

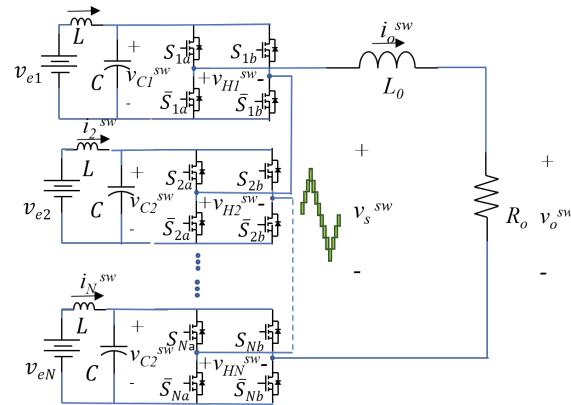


Figure 1. Cascaded Full-Bridge Multilevel Converter of N FBs

Taking into account that the switching current through the output of each Full-Bridge is i_o^{sw} , and the average is i_o for all the FB cells, balancing their output voltage is equivalent to balance the power delivered by each cell. According to Fig. 1, the dynamic equation of the moving average variable is:

$$\dot{i}_k = \frac{1}{L} v_{ek} - R_L \frac{1}{L} i_k - \frac{1}{L} v_{ck} \quad (1a)$$

$$\dot{v}_{C_k} = \frac{1}{C} i_k - \frac{1}{C} u_k i_o \quad (1b)$$

$$\dot{i}_o = \frac{1}{L_o} \sum_{k=1}^N v_{c_k} u_k - \frac{1}{L_o} (R_x + R_o) i_o \quad (1c)$$

where $u_k = d_{ak} - d_{bk}$, d_{yk} is the duty cycle of S_{yk} , R_L is the series resistance of the inductance L , and R_x corresponds to $2NR_{ds} + R_{L_o}$, R_{DS} is the drain-source-ON resistance of the MOSFET and R_{L_o} is the series resistance of L_o . The dynamical model of the output voltage of the Full-Bridge, v_{Hk} is:

$$v_{Hk} = v_{C_k} u_k \quad (2)$$

According to (1) and (2) the equivalent circuit of the converter is shown in Fig. 2:

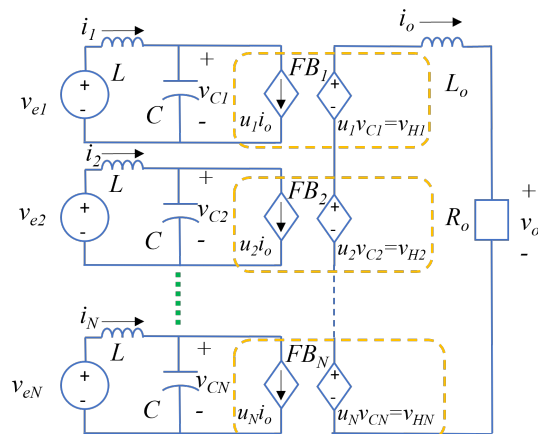


Figure 2. Equivalent circuit of the average model of the Cascaded Multilevel Converter of N FBs

Knowing that in the CFBMC all the input voltages have the same nominal value, $v_{ek} = \bar{v}_e + \hat{v}_{ek}$. Hence, according to [12,26], it is possible to simplify the model, considering the oscillation produced by the input filter and the variations in the input voltage as a disturbance. Therefore:

$$v_{Ck} = \delta_{v_{Ck}} + \bar{v}_e + \hat{v}_{ek} \quad (3)$$

Based on (1c) and (3), the converter follows the presented model:

$$\dot{i}_o = \frac{1}{L_o} \sum_{k=1}^N (\bar{v}_e u_k + \delta_{v_{Hk}}) - \frac{1}{L_o} (R_x + R_o) i_o \quad (4a)$$

$$v_{Hk} = \bar{v}_{ek} u_k + \delta_{v_{Hk}} \quad (4b)$$

where $\delta_{v_{Hk}} = (\delta_{v_{Ck}} + \hat{v}_{ek}) u_k$.

Based on (4), Fig. 3 presents the equivalent linear circuit:

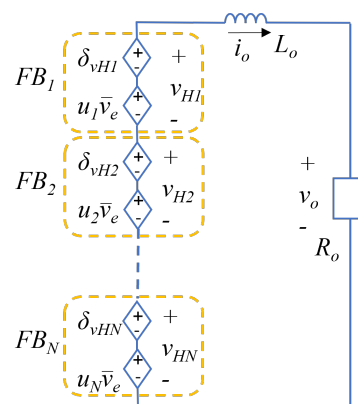


Figure 3. Equivalent circuit of the linear model of the Cascaded Multilevel Converter of N levels

Equation (4) represents the linear model of the inverter. Hence, it is possible to express it in Laplace domain:

$$I_o(s) = \frac{1}{L_o s + (R_x + R_o)} \sum_{k=1}^N (\bar{v}_e U_k(s) + \Delta_{V_{Hk}}(s)) \quad (5a)$$

$$V_{Hk}(s) = \bar{v}_e U_k(s) + \Delta_{V_{Hk}}(s) \quad (5b)$$

Then, expressing it as a matrix form:

$$I_o(s) = G(s) \mathbf{V}_1^T (\bar{v}_e \mathbf{U}(s) + \Delta_{\mathbf{V}_H}(s)) \quad (6a)$$

$$\mathbf{V}_H(s) = \bar{v}_e \mathbf{U}(s) + \Delta_{\mathbf{V}_H}(s) \quad (6b)$$

where $G(s) = \frac{1}{L_o s + (R_x + R_o)}$, $\Delta_{\mathbf{V}_H}(s) = [\Delta_{V_{H1}}(s) \quad \Delta_{V_{H2}}(s) \quad \dots \quad \Delta_{V_{HN}}(s)]^T$,

$\mathbf{U}(s) = [U_1(s) \quad U_2(s) \quad \dots \quad U_N(s)]^T$, $\mathbf{V}_1 = [1 \quad 1 \quad \dots \quad 1]^T$.

Fig. 4 shows the block diagram of (6). Thanks to this model, a decentralized controller used to balance the output voltage of the cells v_{Hk} is proposed in the next chapter.

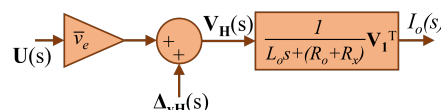


Figure 4. Block diagram of the linear model of the cascaded FB multilevel converter

3. Description of the decentralized controller

The proposed control loop for this article is based on the controller found in [3,21] that is applied to a FCMC, which shows interesting results. Furthermore, [23] shows a simulation of this controller applied in a grid-tied cascaded multilevel inverter. The presented paper implements the controller to an isolated Cascaded FB Multilevel Inverter, connected to a resistive load with an inductive filter. Fig. 5 shows the proposed control structure.

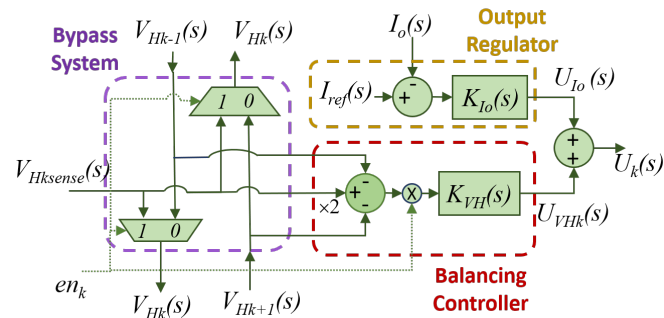


Figure 5. Block diagram of the control system computing the local duty-cycle $U_k(s)$ of the k^{th} cell.

As Fig. 5 shows, the control structure presents three stages: the Bypass system, the Balancing controller and the Output Current regulator.

3.1. The Bypass System

The main goal of this block is to manage the communication between the cells depending on its state (active or inactive, ON or OFF). According to Fig. 5, the cell controller receives an enable signal used to turn OFF or ON the FB cell. When the k^{th} FB cell is ON, the bypass system sends $V_{Hksense}(s)$ to $V_{Hk}(s)$, which is the signal that is sent to the cell $k + 1$ and $k - 1$, respectively. When the k^{th} cell is OFF, the FB is skipped and the value of $V_{Hksense}(s)$ is not sent anymore. Instead of that, the cells $k + 1$ and $k - 1$ receive the values of $V_{Hk-1}(s)$ and $V_{Hk+1}(s)$, respectively. This part of the controller allows the insertion or removal of FB cells during operation. However, if a balancing controller is not implemented, each FB cell can supply different power, voltage, or current that could not be the desired one.

3.2. The Output Current Regulator

This part of the controller regulates the output current supplied to the load. It is a typical linear controller, $K_{Io}(s)$, that can be a PI or other regulator, based on the transfer function of the plant. According to Fig. 5, the output of the output regulator is defined as:

$$U_{Io}(s) = K_{Io}(s)(I_{ref}(s) - I_o(s)) \quad (7)$$

3.3. The Cell Power Balancing Controller

This stage of the control structure is the cell power balancing controller. It compares the values of its output voltage $V_{Hk}(s)$ with the average value of the output voltages of the neighboring actives FB cells, $V_{Hk-1}(s)$ and $V_{Hk+1}(s)$. The error obtained is then canceled by a linear controller, $K_{VH}(s)$, that can be a PI or another type of compensator.

$$U_{VHk}(s) = K_{VH}(s)(2V_{Hk}(s) - V_{Hk+1}(s) - V_{Hk-1}(s)) \quad (8)$$

According to (7), (8) and Fig. 5, the output of the entire controller is defined as:

$$U_k(s) = U_{I_o}(s) + U_{V_{Hk}}(s) \quad (9a)$$

$$U_k(s) = K_{I_o}(s)(I_{ref}(s) - I_o(s)) + K_{V_H}(s)(2V_{Hk}(s) - V_{Hk+1}(s) - V_{Hk-1}(s)) \quad (9b)$$

The control method illustrated in Fig. 5 is applied to each FB cell. Then the cells are connected together in a closed-loop chain of communications to exchange with their close neighbors the values of their output voltage, as shows Fig. 6.

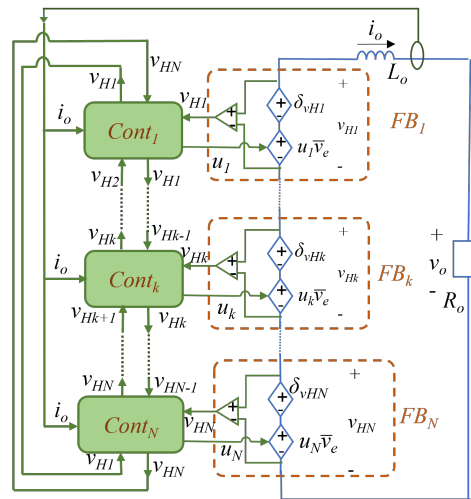


Figure 6. Block diagram of the linear model of the cascaded FB multilevel converter with the proposed controller in closed-loop chain of communication

Notice that the N^{th} cell communicates with the 1^{st} and $N-1^{th}$ cells, and the 1^{st} cells are compared with the cell 2^{nd} and N^{th} , closing the chain of the system.

Expressing (9b) as a matrix form, it follows:

$$\mathbf{U}(s) = K_{I_o}(s)(I_{ref}(s) - I_o(s))\mathbf{V}_1 + K_{V_H}(s)\mathbf{D}_{\text{diff}}\mathbf{V}_H(s) \quad (10)$$

where

$$\mathbf{D}_{\text{diff}} = \begin{bmatrix} 2 & -1 & 0 & \dots & 0 & -1 \\ -1 & 2 & -1 & \ddots & \vdots & 0 \\ 0 & -1 & 2 & \ddots & 0 & \vdots \\ \vdots & 0 & \ddots & \ddots & -1 & 0 \\ 0 & \vdots & \ddots & -1 & 2 & -1 \\ -1 & 0 & \dots & 0 & -1 & 2 \end{bmatrix}$$

4. Closed-Loop System Analysis

This section shows the mathematical study of the closed-loop system using the proposed controller. The analysis of the transfer functions which comprise the output current regulator and the local balancing controller makes it possible to determine the nature and the parameters of the controllers used. Their design is discussed in the next chapter. The block diagram of the system, and the model of the converter with the controllers is shown in Fig. 7.

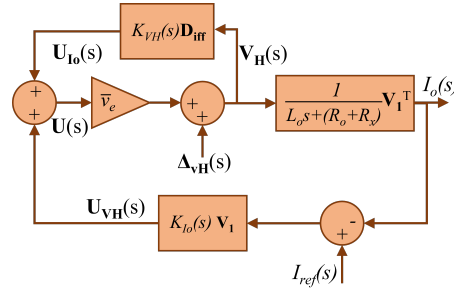


Figure 7. Block diagram of the Closed-Loop system with the proposed controller

Thanks to Fig. 7, one can determine the open-loop transfer function and the closed-loop transfer function of the output regulator and the ones of the balancing controller.

4.1. Output Current Regulator Analysis

To design the output regulator it is necessary to perform an analyzes the output regulator loop. Hence, inserting the decentralized controller, proposed in (10), into the model of the output current control loop of the inverter, and taking into account that $\mathbf{V}_1^T \mathbf{V}_1 = N$ and $\mathbf{V}_1^T \mathbf{D}_{\text{diff}} = 0$, (6a) one obtains:

$$I_o(s) = \underbrace{\frac{N \bar{v}_e K_{I_o}(s)}{L_o s + R_{x_o}}}_{F_{olI_o}(s)} (I_{ref}(s) - I_o(s)) + \frac{1}{L_o s + R_{x_o}} \mathbf{V}_1^T \Delta \mathbf{V}_H(s) \quad (11)$$

where $R_{x_o} = R_x + R_o$ and $F_{olI_o}(s)$ is the open-loop transfer function of the output current regulator.

Notice that the term related to the balancing control stage is removed in the transfer function because \mathbf{D}_{diff} represents the Laplacian of a graph. Indeed, according to [3,21,23], the sum of the elements of the rows and the sum of the elements of the columns is zero. Because this matrix is post multiplied by \mathbf{V}_1 , the results are zero. Based on $F_{olI_o}(s)$, the design of $K_{I_o}(s)$ is provided in the next section.

In order to get a better understanding of the balancing control loop, it is necessary to analyze the closed-loop transfer function of the output regulator, $F_{clI_o}(s)$, which is defined below.

$$I_o(s) = \underbrace{\frac{N \bar{v}_e K_{I_o}(s)}{L_o s + R_{x_o} + N \bar{v}_e K_{I_o}(s)}}_{F_{clI_o}(s)} I_{ref}(s) + \underbrace{\frac{1}{L_o s + R_{x_o} + N \bar{v}_e K_{I_o}(s)}}_{F_{dist}(s)} \mathbf{V}_1^T \Delta \mathbf{V}_H(s) \quad (12)$$

It shows that the resulting regulated output current is provided by the separate contribution of the current loop $F_{clI_o}(s)$ and a disturbance transfer function, $F_{dist}(s)$, generated by the oscillations of the input voltage capacitors and the duty cycles of each cell FB.

For the next subsection it should be considered if the output regulator is well designed, when $I_{ref}(s)$ is a step, $I_{ref}(s) = \frac{I_a}{s}$ at $t \rightarrow \infty$, means that with $s \rightarrow 0$, $i_o(t) = I_a$, producing that $F_{clI_o}(s) = 1$ when $s \rightarrow 0$.

4.2. Cell Power Balancing Control loop analysis

Now, the balancing control loop has to be analyzed Inserting (10) in (6b), it follows:

$$\mathbf{V}_H(s) = \bar{v}_e K_{V_H}(s) \mathbf{D}_{\text{diff}} \mathbf{V}_H(s) + \bar{v}_e K_{I_o}(s) (I_{ref}(s) - I_o(s)) \mathbf{V}_1 + \Delta \mathbf{V}_H(s) \quad (13)$$

Inserting (12) in (13), one obtains

$$\begin{aligned} \mathbf{V}_{\mathbf{H}}(s) = & \bar{v}_e K_{V_H}(s) \mathbf{D}_{\text{iff}} \mathbf{V}_{\mathbf{H}}(s) + \frac{\bar{v}_e K_{I_o}(s)(L_o s + R_{xo})}{L_o s + R_{xo} + N \bar{v}_e K_{I_o}(s)} I_{ref}(s) \mathbf{V}_1 \\ & + \left(\mathbb{I} - \frac{\bar{v}_e K_{I_o}(s)}{L_o s + R_{xo} + N \bar{v}_e K_{I_o}(s)} \mathbf{V}_1 \mathbf{V}_1^T \right) \Delta \mathbf{V}_{\mathbf{H}}(s) \end{aligned} \quad (14)$$

Simplifying:

$$\begin{aligned} \mathbf{V}_{\mathbf{H}}(s) = & \underbrace{\bar{v}_e K_{V_H}(s) \mathbf{D}_{\text{iff}}}_{\mathbf{F}_{olV_H}(s)} \mathbf{V}_{\mathbf{H}}'(s) + \frac{1}{N} F_{clI_o}(s)(L_o s + R_{xo}) I_{ref}(s) \mathbf{V}_1 \\ & + \left(\mathbb{I} - \frac{1}{N} F_{clI_o}(s) \mathbf{V}_1 \mathbf{V}_1^T \right) \Delta \mathbf{V}_{\mathbf{H}}(s) \end{aligned} \quad (15)$$

where $\mathbf{V}_{\mathbf{H}}'(s)$ is the excitation signal. The controller $K_{V_H}(s)$ is defined based on the desired bandwidth of $F_{olV_H}(s)$, which is directly linked to the eigenvalues of the matrix \mathbf{D}_{iff} , then it is described in the next section.

4.3. Global closed-loop analysis

According to (11), and (13), Fig. 8 shows the simplified closed-loop block diagram.

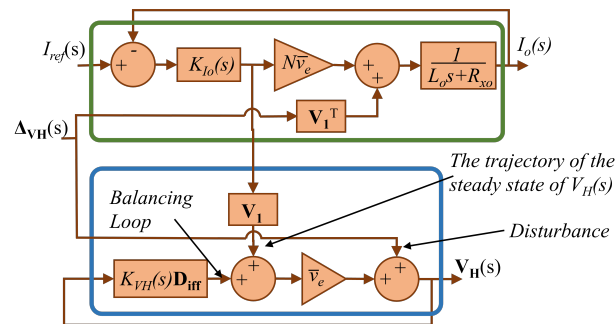


Figure 8. Simplified closed-loop transfer function of the system

Notice that $\mathbf{V}_{\mathbf{H}}(s)$ depends on three inputs, one corresponds to the balancing controller, other depends on the disturbance, $\Delta \mathbf{V}_{\mathbf{H}}(s)$, and the last one depends on the output current loop, which affects all the cell voltages at the same time. Analyzing in steady state, according to (15), when $s \rightarrow 0$, if the controller is well designed, $F_{clI_o}(s) = 1$, producing that the trajectory in steady states for $\mathbf{V}_{\mathbf{H}}(s)$ is $\frac{R}{N} I_{ref}(s)$.

5. Design of the controllers

Now, both controllers have to be designed, taking into account some criteria, such as bandwidth of the loops and the correlation of Bode analysis between the two loops.

5.1. Design of the Output Current Regulator

Based on $F_{olI_o}(s)$, for a stable and low bandwidth system, an integral corrector can be proposed for $K_{I_o}(s)$, and the chosen controller type for the output current regulator is an Integral (I) controller, hence:

$$K_{I_o}(s) = k_i \frac{1}{s} \quad (16)$$

The Bode analysis of $F_{olI_o}(s)$, $K_{I_o}(s)$ and $G(s)$ are shown in Fig. 9:

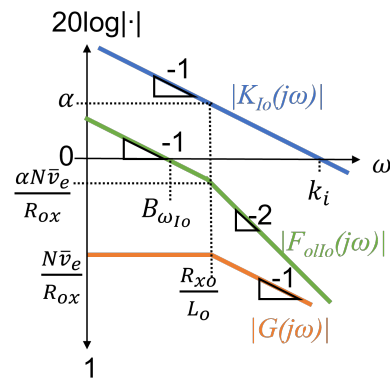


Figure 9. Bode diagram of $G(s)$, $K_{VH}(s)$ and $F_{olIo}(s)$

According to Fig. 9, it follows:

$$\alpha = \frac{k_i L_o}{R_{xo}} \quad (17a)$$

$$\frac{\alpha N \bar{v}_e}{R_{xo}} = \frac{B_{\omega Io} L_o}{R_{xo}} \quad (17b)$$

$$k_i = \frac{B_{\omega Io} R_{xo}}{N \bar{v}_e} \quad (17c)$$

where $B_{\omega Io}$ is the bandwidth of the output regulator, which is fixed ten time less than the switching frequency of the MOSFETs, f_{sw} . 183
184

5.2. Design of the cell power balancing controllers 185

The balancing controller is designed based on the $F_{olVH}(s)$ expression. According to (15), $\mathbf{F}_{olVH}(s) = \bar{v}_e K_{VH}(s) \mathbf{D}_{\text{iff}}$. Then, decomposing \mathbf{D}_{iff} in its modal and diagonal matrix, $\mathbf{F}_{olVH}(s)$ follows to:

$$\mathbf{D}_{\text{iff}} = \mathbf{V}_{\text{eig}} \mathbf{\Lambda} \mathbf{V}_{\text{eig}}^{-1} \quad (18a)$$

$$\mathbf{F}_{olVH}(s) = \mathbf{V}_{\text{eig}} \underbrace{\bar{v}_e K_{VH}(s) \mathbf{\Lambda}}_{\mathbf{\Pi}(s)} \mathbf{V}_{\text{eig}}^{-1} \quad (18b)$$

where $\mathbf{\Lambda}$ and \mathbf{V}_{eig} are the Diagonal and Modal matrix of \mathbf{D}_{iff} , respectively. It should be noted that one eigenvalue of \mathbf{D}_{iff} is equal to 0, because it is a Laplacian of a graph.

$$\mathbf{\Lambda} = \begin{bmatrix} \lambda_1 & 0 & \dots & 0 \\ 0 & \lambda_2 & \ddots & \vdots \\ \vdots & \ddots & \ddots & 0 \\ 0 & \dots & 0 & \lambda_N \end{bmatrix}; \lambda_1 = 0 \quad (19)$$

$\mathbf{\Pi}(s)$ represents the transfer function of the modal response, defined as:

$$\mathbf{\Pi}(s) = K_{VH}(s) \begin{bmatrix} p_1(s) & 0 & \dots & 0 \\ 0 & p_2(s) & \ddots & \vdots \\ \vdots & \ddots & \ddots & 0 \\ 0 & \dots & 0 & p_N(s) \end{bmatrix} \quad (20)$$

where $p_k(s) = \bar{v}_e \lambda_k$.

Hence the open-loop transfer function of the k^{th} mode is:

$$F_{olm_k}(s) = \bar{v}_e \lambda_k K_{VH}(s) \quad (21)$$

It should be mentioned that \mathbf{D}_{iff} corresponds to a circulant matrix \mathbf{M}_C , which is described as:

$$\mathbf{M}_C = \begin{bmatrix} c_1 & c_2 & \cdots & c_N \\ c_N & c_1 & \ddots & \vdots \\ \vdots & \ddots & \ddots & c_2 \\ c_2 & \cdots & c_N & c_1 \end{bmatrix} \quad (22)$$

Since \mathbf{D}_{iff} is a circulant matrix, it is possible to obtain an expression of its eigenvalues. According to [27] the eigenvalues of a circulant matrix are:

$$\lambda_k = \sum_{n=1}^N c_n e^{j \frac{2\pi(n-1)(k-1)}{N}} \quad (23)$$

where $\hat{j} = \sqrt{-1}$.

It can be observed that for the case of the \mathbf{D}_{iff} , the coefficients, c_n s, are:

$$c_n = \begin{cases} 2 & ; n = 1 \\ -1 & ; n = \{2, N\} \\ 0 & ; n = \{3, 4, \dots, N-1\} \end{cases} \quad (24)$$

Therefore, according to (23) and (24), the eigenvalues of \mathbf{D}_{iff} are defined as:

$$\begin{aligned} \lambda_k &= c_1 + c_2 e^{\frac{2\pi(k-1)}{N} \hat{j}} + c_N e^{\frac{2\pi(k-1)(N-1)}{N} \hat{j}} \\ \lambda_k &= 2 \left(1 - \cos \left(\frac{2\pi(k-1)}{N} \right) \right) \end{aligned} \quad (25)$$

Notice that the first eigenvalue, λ_1 , is equal to 0, validating that it also represents the Laplacian of a graph. Furthermore, because of the symmetric property of the cosine, the k^{th} eigenvalue is equal to the $(N+1-k)^{th}$ eigenvalue. Finally, the highest eigenvalue is obtained for $k = \frac{N}{2} + 1$ when N is even, and $k = \frac{N \pm 1}{2} + 1$ when N is odd. The maximum case is produced when N is even, generating a $\lambda_{max} = 4$. For odd values of N the highest eigenvalue tends to be 4 when N increases. The design of the balancing controller is based on the possible maximum eigenvalue, λ_{max} , and the minimum eigenvalue, $\lambda_{min} = \lambda_1$, which values are 4 and 0, respectively.

$\lambda_{min} = 0$ means the system presents a pure integrator that theoretically is stable. However, because of numeric approximations in the implementation, the system may be unstable after a long lapse. For that reason, the selected controller corresponds to a low-pass filter that ensures the stability of the system, with a pole located at a very low frequency. Hence, the proposed controller is:

$$K_{VH}(s) = k_{pV} \left(\frac{k_{iV}}{s + k_{iV}} \right) \quad (26)$$

In order to determine the parameters of the controller, Fig. 10 shows the Bode diagram of $K_{VH}(s)$, $p_k(s)$, $f_{olm_k}(s)$.

Based on the Bode diagram of Fig. 10, the bandwidth B_{ω_V} is set using the k_{pV} parameter:

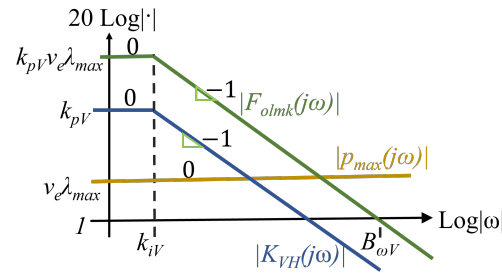


Figure 10. Bode diagram of p_{max} , $K_{VH}(s)$ and $F_{olmk}(s)$ of the CFBC

$$\begin{aligned} v_e \lambda_{max} k_{pV} &= \frac{B_{\omega V}}{k_{iV}} \\ k_{pV} &= \frac{B_{\omega V}}{v_e \lambda_{max} k_{iV}} \end{aligned} \quad (27)$$

The bandwidth, $B_{\omega V}$, must be ten times less than the switching frequency $2\pi f_{sw}$. Due to that, the converter can work either as an inverter, or as a DC/DC converter, the pole k_{iV} is selected ten times less than the operating frequency of the inverter.

6. Results

A prototype implements the proposed decentralized controller is now considered. It has been carried out in the laboratory for measurement purpose. The controllers are implemented in a Cascaded Multilevel Inverter of 5 FBs, as shown in Fig. 11.

Both simulation and experimental results, developed hereafter, are obtained with the converter working as a DC/AC converter, with three different tests: an input voltage step, a load step and a cell insertion during operation. Furthermore, a modal response simulation is also presented. The parameters of the controllers are shown in Table 1:

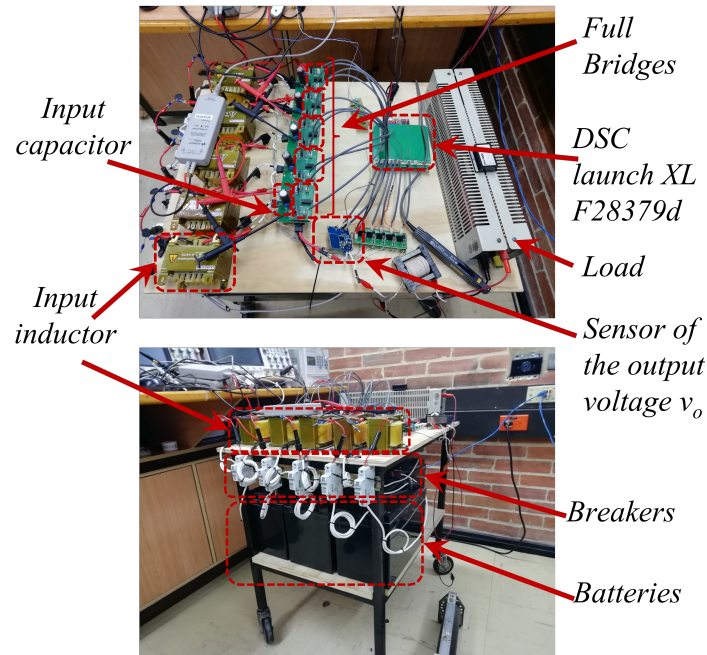


Figure 11. Setup of the Cascaded Full-Bridge Multilevel Inverter

Table 1. Parameters of the CFBMC

Parameter	Value
Number of FBs N	5
Input Voltage (v_e)	48 V
Input Inductance (L)	1.8 mH
ESR of L (R)	200 mΩ
Input Capacitance (C)	4 mF
Drain-Source ON Resistance (R_{DS})	58 mΩ
Frequency of the inverter (f)	60 Hz
I_{ref} as an inverter	1.7 sin(2πft) A
I_{ref} as a DC/DC converter	1.7 A
Switching frequency (f_{sw})	12.5 kHz
Load Resistance (R_o)	60 Ω – 100 Ω
k_i	1884 A ⁻¹ s ⁻¹
k_{pV}	39 V ⁻¹ s ⁻¹
k_{iV}	37.7 rads/s

6.1. Modal Response Simulation

This simulation corresponds to the modal respond of the transfer function of the balancing loop. For $N = 5$, $\mathbf{\Lambda}$ corresponds to:

$$\mathbf{\Lambda} = \frac{\sqrt{5}}{2} \begin{bmatrix} 0 & 0 & 0 & 0 & 0 \\ 0 & \sqrt{5}-1 & 0 & 0 & 0 \\ 0 & 0 & \sqrt{5}+1 & 0 & 0 \\ 0 & 0 & 0 & \sqrt{5}+1 & 0 \\ 0 & 0 & 0 & 0 & \sqrt{5}-1 \end{bmatrix} \quad (28)$$

Appendix 1 shows the demonstration of these values, which their numeric values are: $[\lambda_1 \ \lambda_2 \ \lambda_3 \ \lambda_4 \ \lambda_5]^T = [0 \ 1.38 \ 3.62 \ 3.62 \ 1.38]^T$ while the modal matrix, \mathbf{V}_{eig} , is:

$$\mathbf{V}_{\text{eig}} = \begin{bmatrix} 1.00 & 1.00 & 1.00 & 1.00 & 1.00 \\ 1.00 & -0.57 & -0.52 & -2.00 & 1.33 \\ 1.00 & -1.35 & -0.16 & 2.23 & -0.18 \\ 1.00 & -0.26 & 0.78 & -1.61 & -1.44 \\ 1.00 & 1.19 & -1.1 & 0.38 & -0.72 \end{bmatrix} \quad (29)$$

$\underbrace{\mathbf{V}_{\text{eig}}(\lambda_1)} \quad \underbrace{\mathbf{V}_{\text{eig}}(\lambda_2)} \quad \underbrace{\mathbf{V}_{\text{eig}}(\lambda_3)} \quad \underbrace{\mathbf{V}_{\text{eig}}(\lambda_4)} \quad \underbrace{\mathbf{V}_{\text{eig}}(\lambda_5)}$

Using the eigenvectors as the initial conditions, Fig. 12 shows the modal respond of the system.

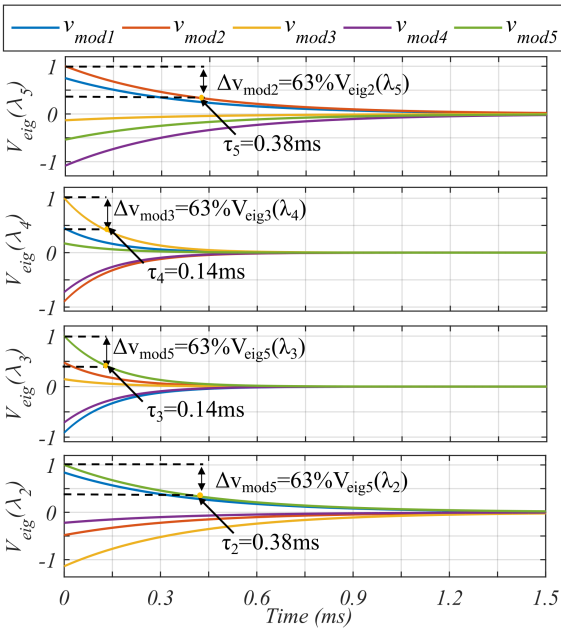


Figure 12. Modal response of the of the CFBMC with the decentralized controller

It is clearly observed that the system is stable and the time response of the modes are very different. Depending on the parameter k_{pV} of the decentralized controller, this time response can be adjusted. Table 2 shows a comparison between the theoretical time constants and the ones obtained by simulation.

Table 2. Time constants of the CFBMC

τ_k	Theoretical (ms)	Simulated (ms)
τ_2	0.384	0.38
τ_3	0.146	0.14
τ_4	0.146	0.14
τ_5	0.384	0.38

Notice that given that there are two pairs of similar eigenvalues, there are also two pairs of time constants, meaning that there are two double poles at these time constants. Furthermore, it can be observed that simulated and theoretical values are very similar, validating the performance of the controller.

6.2. Full System Simulation Results

The first simulation test corresponds to a load transient from 95 Ω to 70 Ω . Fig. 13 shows v_s and i_o when the converter works as a DC/AC converter.

It is observed that before the disturbance occurs, the multilevel converter uses 9 voltage levels. After the disturbance, only 7 levels are required to regulate the output current. Notice also that the CVs are balanced during all the simulation, before and after the disturbance, validating for DC/AC conversion that when a disturbance in the output current occurs, the CVs are not unbalanced, only their common average value are affected. Furthermore, the current is stabilized during a small transient, less than 1 ms.

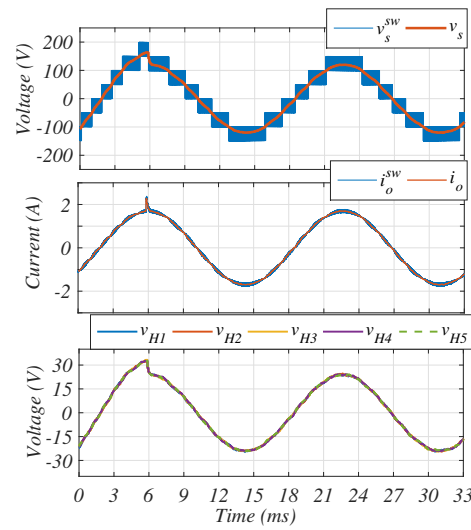


Figure 13. Load transient test as a DC/AC converter

The next simulation result, shown in Fig. 14, corresponds to an input cell voltage disturbance, i.e. a step voltage from 40 to 50V for the inverter with a resistive load of 77 Ω .

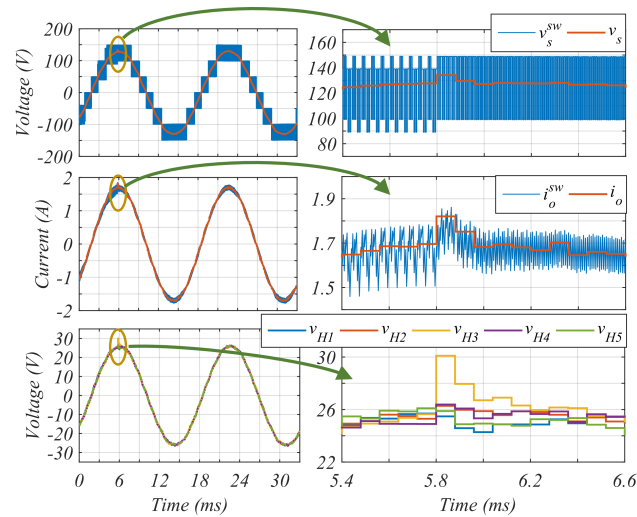


Figure 14. Input cell voltage step response simulation for the inverter case

It should be noted that the voltage disturbance almost affects neither the output current i_o nor the output voltage v_s , while the CVs are automatically balanced thanks to the decentralized controllers in only 0.5 ms. Fig. 14 also shows that, by nature of the inverter, when one of the input voltages is 40 V, there exists an asymmetric ripple in i_o^{sw} and v_s^{sw} and when the input voltage is 50 V, the ripples are equalized. However, in both cases the average output current i_o and the v_{Hk} s are well regulated and balanced, respectively.

The next simulation corresponds to a cell insertion during operation, going from 4 FBs to 5 FBs, when the converter operates as an inverter. Fig. 15 shows the results obtained for the v_{Hk} s, i_o and v_s signals.

It should be noticed that before the cell insertion, i_o and v_s present both a high ripple, due to a constant control signal interleaving set for 5 cells, i.e. signal phase. Even if the ripple is high, the average value of the output current is regulated when only 4 cells are activated. When the fifth FB cell is inserted, i_o presents an overshoot and then it is stabilized in less than 0.25 ms. v_{Hk} s voltages are balanced when there are 4 FBs and then, when the 5th cell is inserted, there are auto balanced, reaching a new operation point in 0.25 ms approximately.

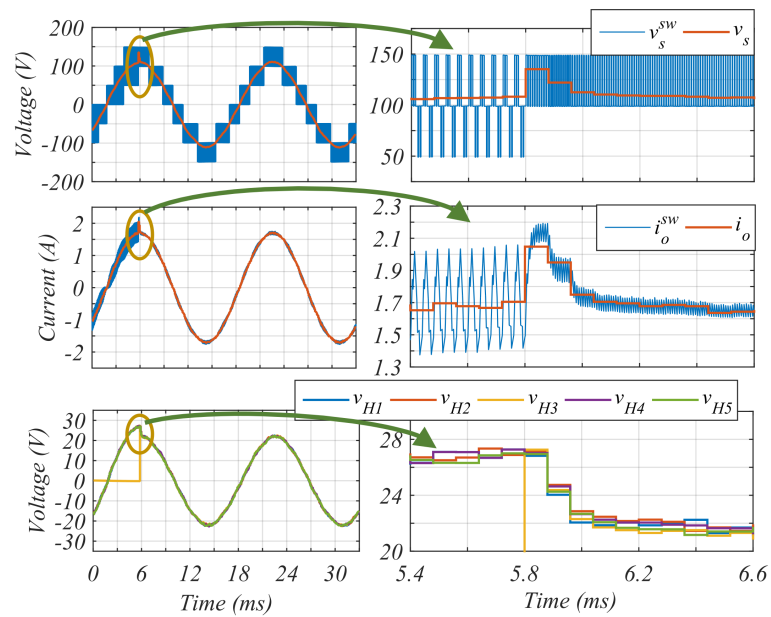


Figure 15. FB insertion simulation for blue the inverter case

This test validates by simulation the three functions of the controller, the balancing of the CV, the regulation of the GV, and the bypass system activation. It can be inferred that all the simulation results are in concordance with the previous theoretical study, producing the expected behavior in terms of reconfigurability, bandwidth and stability for this multilevel converter topology.

6.3. Experimental Results

The experimental results are developed with a prototype composed of a CFBMC of 5 FB, fed by Li-ion Batteries of 48 V, with the parameters described in table 1. More details related to the construction of the inverter is presented in [28].

In order to compare the simulation and experimental results, the tests developed here are the same than the ones illustrated in the previous simulations.

Fig. 16 shows the experimental results of first test, corresponding to a load step (or load transient). It can be seen that there exists a concordance with the simulation result of this test, presenting similar overshoot in the current and similar settling time. Moreover, the switching levels of v_s are the same. Furthermore, as happened in the simulation, the operating points of v_{Hk} s change in 0.5 ms without any unbalance between them.

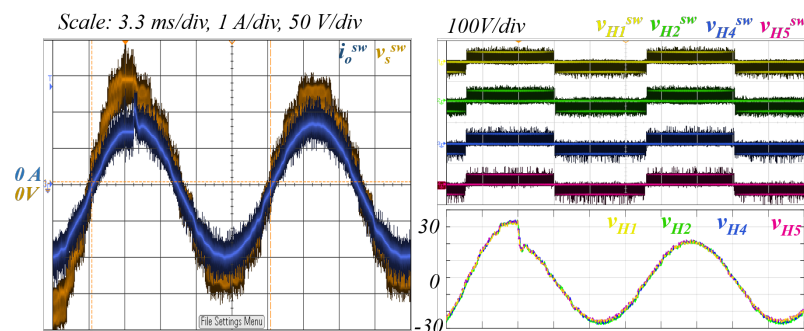


Figure 16. Load transient experimental test in DC/AC mode

The next result corresponds to the disturbance in one input voltage FB cell. Fig. 17 shows the behavior of the output current i_o^{sw} , the output voltage v_s^{sw} , the switching output voltage of each FB 1, 4 and 5, v_{Hk}^{sw} , $\forall k = \{1, 4, 5\}$, and their respectively moving average, v_{HkS} .

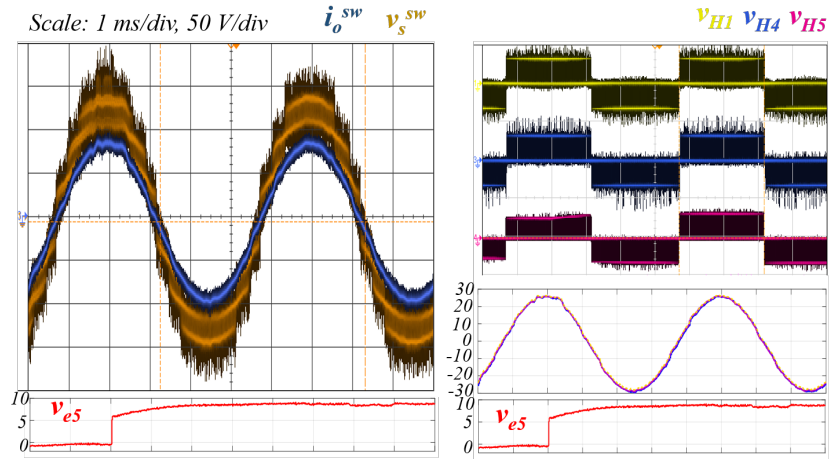


Figure 17. Input cell voltage disturbance experimental test.

It should be noted that the step voltage is almost not detected in v_{Hs} . This is because the input filters presented in the converter smooth the effect of the voltage disturbance. Furthermore, it can be observed that during all the experiments v_{HkS} voltage are well balanced. This observation also validates the balancing controller, maintaining the same output voltage of each FB cell even when the input voltages change. Additionally, the output current is well regulated.

The next result, presented in Fig. 18, corresponds to a FB cell insertion during operation, starting with 4 FB cell and inserting the 5th FB cell. It is important to note that the current follows the reference during all the experiments, presenting a small transient when the FB cell is inserted. Furthermore, it can be observed that the CVs are well balanced after the insertion, reaching a new operating point with a settling time of 0.6 ms, approximately. These values are in concordance with the predicted time constants of the system and show a strong similarity with the simulation results. This test validates the three stages of the controller, the balancing controller, the GV regulator, and the bypass system.

It can be inferred that all the experimental tests are in concordance with the simulation tests and the theoretical studies developed in this paper, demonstrating the good performance of the controller for this topology.

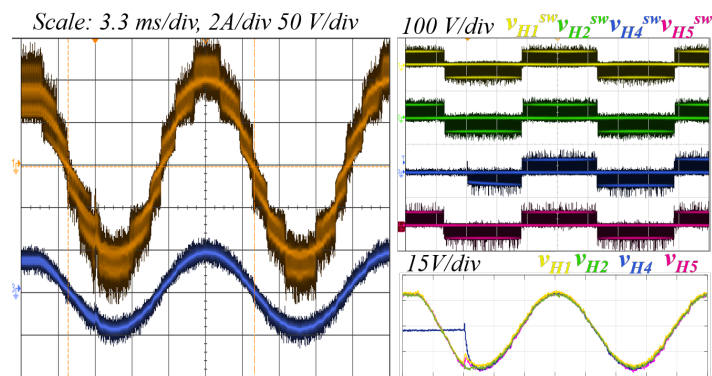


Figure 18. FB cell insertion experimental test in DC/AC mode

7. Conclusion

A decentralized control principle for the balancing of the power delivered by the FB cell of a multilevel converter has been shown in this paper.

The decentralized control is composed of several controllers, each associated with a cell of the inverter, which adjust their local control signal by comparing their sensed cell voltage with those of the closest neighbors.

This control method can handle a huge number of cells and makes it possible to obtain a robust system for the case of load transient and cell battery voltages variations.

Moreover, it allows to manage the number of active cells and to carry out reconfiguration during operation. These reconfiguration capability can be useful in case of a cell failure and address functional safety concerns.

Tests of a laboratory prototype help to demonstrate the robustness of the proposed method.

Two future works are in mind with this control method. The first one is the implementation of this controller for balancing the state of charge of the batteries that are the input sources of a CF BMC, and the second future work is the implementation of this control method in a multi-phase buck converter.

8. Appendix

8.1. Appendice 1: Demonstration of the eigenvalues

For $N = 5$, the eigenvalues are:

$$\begin{aligned}\lambda_1 &= 2(1 - \cos(0)) \\ \lambda_2 &= 2(1 - \cos(\frac{2\pi}{5})) \\ \lambda_3 &= 2(1 - \cos(\frac{4\pi}{5})) \\ \lambda_4 &= 2(1 - \cos(\frac{6\pi}{5})) \\ \lambda_5 &= 2(1 - \cos(\frac{8\pi}{5}))\end{aligned}$$

Using trigonometric identities, follows to:

$$\begin{aligned}\lambda_1 &= 0 \\ \lambda_2 &= 2(1 - \cos(\frac{2\pi}{5})) \\ \lambda_3 &= 2(1 + \cos(\frac{\pi}{5})) \\ \lambda_4 &= 2(1 + \cos(\frac{\pi}{5})) \\ \lambda_5 &= 2(1 - \cos(\frac{2\pi}{5}))\end{aligned}$$

assigning $\alpha = \cos(\pi/5)$, and using trigonometric identities follows:

$$\begin{aligned}\lambda_1 &= 0 \\ \lambda_2 &= 4(1 - \alpha^2) \\ \lambda_3 &= 2(1 + \alpha) \\ \lambda_4 &= 2(1 + \alpha) \\ \lambda_5 &= 4(1 - \alpha^2)\end{aligned}$$

Hence, obtaining α all the eigenvalues are found. Taking into account that $\cos(\frac{\pi}{2}) = 0$, $\cos(2\frac{\pi}{5} + (\frac{1}{2})\frac{\pi}{5}) = 0$, hence:

$$\cos(2\frac{\pi}{5}) \cos((\frac{1}{2})\frac{\pi}{5}) - \sin(2\frac{\pi}{5}) \sin((\frac{1}{2})\frac{\pi}{5}) = 0$$

Using the double and half angle formulas and taking into account that $\alpha = \cos(\frac{\pi}{5})$ follows:

$$(2\alpha^2 - 1) \frac{\sqrt{1+\alpha}}{\sqrt{2}} - 2\alpha \sqrt{1-\alpha^2} \frac{\sqrt{1-\alpha}}{\sqrt{2}} = 0$$

$$(\sqrt{1+\alpha})(2\alpha^2 - 1 - 2\alpha(1-\alpha)) = 0$$

$$(\sqrt{1+\alpha})(4\alpha^2 - 2\alpha - 1) = 0$$

$\alpha = -1$ ✗ because it produces an angle of $\pi/2$

$\alpha = \frac{1-\sqrt{5}}{4}$ ✗ because α should be positive

$$\alpha = \frac{1+\sqrt{5}}{4} \checkmark$$

Hence:

$$\lambda_1 = 0$$

$$\lambda_2 = \frac{\sqrt{5}}{2}(\sqrt{5} - 1)$$

$$\lambda_3 = \frac{\sqrt{5}}{2}(\sqrt{5} + 1)$$

$$\lambda_4 = \frac{\sqrt{5}}{2}(\sqrt{5} + 1)$$

$$\lambda_5 = \frac{\sqrt{5}}{2}(\sqrt{5} - 1)$$

References

1. Mohan, N.; Undeland, T.; Robbins, W.P. Power Electronics: Converters, Applications and Design. 1989. 321
2. Rashid, M.H. *Power electronics: devices, circuits and applications*; Pearson, 2014. 322
3. Vivert, M.; Cousineau, M.; Ladoux, P.; Fabre, J. Decentralized Controller for the Cell-Voltage Balancing of a Multilevel Flying Cap Converter. In Proceedings of the PCIM Europe 2019; International Exhibition and Conference for Power Electronics, Intelligent Motion, Renewable Energy and Energy Management, 2019, pp. 1–8. 323
4. Fabre, J.; Ladoux, P.; Solano, E.; Gateau, G.; Blaqui re, J. Full SiC multilevel chopper for three-wire supply systems in DC electric railways. In Proceedings of the 2016 International Conference on Electrical Systems for Aircraft, Railway, Ship Propulsion and Road Vehicles International Transportation Electrification Conference (ESARS-ITEC), 2016, pp. 1–7. <https://doi.org/10.1109/ESARS-ITEC.2016.7841371>. 324
5. Fabre, J.; Ladoux, P.; Solano, E.; Gateau, G.; Blaqui re, J. MVDC Three-Wire Supply Systems for Electric Railways: Design and Test of a Full SiC Multilevel Chopper. *IEEE Transactions on Industry Applications* **2017**, *53*, 5820–5830. <https://doi.org/10.1109/TIA.2017.2747498>. 325
6. Meynard, T.A.; Foch, H. Multi-level conversion: high voltage choppers and voltage-source inverters. In Proceedings of the PESC '92 Record. 23rd Annual IEEE Power Electronics Specialists Conference, 1992, pp. 397–403 vol.1. <https://doi.org/10.1109/PESC.1992.254717>. 326
7. Meynard, T.A.; Fadel, M.; Aouda, N. Modeling of multilevel converters. *IEEE Transactions on Industrial Electronics* **1997**, *44*, 356–364. <https://doi.org/10.1109/41.585833>. 327
8. Negash, M.F.; Manthathi, U.B. Development of 7-level cascaded H-bridge inverter topology for PV applications. In Proceedings of the International Conference on Electrical, Electronics, and Optimization Techniques, ICEEOT 2016; IEEE: Chennai, Tamil Nadu, India, 2016; pp. 1847–1852. <https://doi.org/10.1109/ICEEOT.2016.7755008>. 328
9. Vivert, M.; Diez, R.; Cousineau, M.; Bernal Cobaleda, D.; Patino, D.; Ladoux, P. Real-Time Adaptive Selective Harmonic Elimination for Cascaded Full-Bridge Multilevel Inverter. *Energies* **2022**, *15*. <https://doi.org/10.3390/en15092995>. 329
10. Luo, F.L.; Ye, H. Multilevel DC/AC Inverters. In *Advanced DC/AC Inverters: Applications in Renewable Energy*; CRC Press: Boca Raton, FL, 2013; chapter 8, pp. 137–154. 330
11. Luo, F.L.; Ye, H. Trinary Hybrid Multilevel Inverters. In *Advanced DC/AC Inverters: Applications in Renewable Energy*; CRC Press: Boca Raton, FL, 2013; chapter 9, pp. 155–205. 331
12. Vivert, M.; Patino, D.; Diez, R. Modulation Strategy and Controller for Grid-Tied Trinary Hybrid Multilevel Inverter. *IEEE Journal of Emerging and Selected Topics in Power Electronics* **2019**, pp. 1–1. <https://doi.org/10.1109/JESTPE.2019.2942325>. 332

13. Liu Yu, F.L. Trinary hybrid 81-level multilevel inverter for motor drive with zero common-mode voltage. *IEEE Transactions on Industrial Electronics* **2008**, *55*, 1014–1021. <https://doi.org/10.1109/TIE.2007.909072>.

14. Cousineau, M.; Cougo, B. Interleaved converter with massive parallelization of high frequency GaN switching-cells using decentralized modular analog controller. In Proceedings of the 2015 IEEE Energy Conversion Congress and Exposition (ECCE), 2015, pp. 4343–4350. <https://doi.org/10.1109/ECCE.2015.7310274>.

15. Le Bolloch, M.; Cousineai, M.; Meynard, T. New Masterless Modular Current-Sharing technique for DC/DC Parallel converters. In Proceedings of the Proceedings of 14th International Power Electronics and Motion Control Conference EPE-PEMC 2010, 2010, pp. T3–73–T3–80. <https://doi.org/10.1109/EPEPEMC.2010.5606884>.

16. Fabre, J.; Ladoux, P. Parallel Connection of 1200-V/100-A SiC-MOSFET Half-Bridge Modules. *IEEE Transactions on Industry Applications* **2016**, *52*, 1669–1676. <https://doi.org/10.1109/TIA.2015.2496109>.

17. Sahoo, S.K.; Bhattacharya, T. Phase-Shifted Carrier-Based Synchronized Sinusoidal PWM Techniques for a Cascaded H-Bridge Multilevel Inverter. *IEEE Transactions on Power Electronics* **2018**, *33*, 513–524. <https://doi.org/10.1109/TPEL.2017.2669084>.

18. Huang, Q.; Q. Huang, A. Feedforward Proportional Carrier-Based PWM for Cascaded H-Bridge PV Inverter. *IEEE Journal of Emerging and Selected Topics in Power Electronics* **2018**, *6*, 2192–2205. <https://doi.org/10.1109/JESTPE.2018.2817183>.

19. Tengfei Wang.; Yongqiang Zhu. Analysis and comparison of multicarrier PWM schemes applied in H-bridge cascaded multi-level inverters. In Proceedings of the 2010 5th IEEE Conference on Industrial Electronics and Applications, 2010, pp. 1379–1383. <https://doi.org/10.1109/ICIEA.2010.5514885>.

20. Arazm, S.; Vahedi, H.; Al-Haddad, K. Phase-shift modulation technique for 5-level packed U-cell (PUC5) inverter. In Proceedings of the 2018 IEEE 12th International Conference on Compatibility, Power Electronics and Power Engineering (CPE-POWERENG 2018), 2018, pp. 1–6. <https://doi.org/10.1109/CPE.2018.8372577>.

21. Vivert, M.; Cousineau, M.; Ladoux, P.; Fabre, J.; Mannes-Hillesheim, M.; Diez, R.; Patino, D. Decentralized Control for Balancing the Cell Voltages of a High Conversion Ratio Flying Capacitor Multilevel Converter. *IEEE Journal of Emerging and Selected Topics in Industrial Electronics* **2022**, *3*, 635–646. <https://doi.org/10.1109/JESTIE.2021.3115958>.

22. Xu, B.; Tu, H.; Du, Y.; Yu, H.; Liang, H.; Lukic, S. A Distributed Control Architecture for Cascaded H-Bridge Converter. In Proceedings of the 2019 IEEE Applied Power Electronics Conference and Exposition (APEC), 2019, pp. 3032–3038. <https://doi.org/10.1109/APEC.2019.8722268>.

23. M. Vivert, D. Patino, R.D.D.B.; Cousineau, M. Decentralized Controller for a Grid Tied Cascade Multilevel Invert. In Proceedings of the IEEE 3rd Colombian Conference on Automatic Control (CCAC), 2019.

24. Achanta, P.K.; Maksimovic, D.; Ilic, M. Decentralized control of series stacked bidirectional DC-AC modules. In Proceedings of the 2018 IEEE Applied Power Electronics Conference and Exposition (APEC), 2018, pp. 1008–1013. <https://doi.org/10.1109/APEC.2018.8341138>.

25. He, J.; Li, Y.; Liang, B.; Wang, C. Inverse Power Factor Droop Control for Decentralized Power Sharing in Series-Connected-Microconverters-Based Islanding Microgrids. *IEEE Transactions on Industrial Electronics* **2017**, *64*, 7444–7454. <https://doi.org/10.1109/TIE.2017.2674588>.

26. Vivert, M.; Patino, D.; Diez, R. Variation of a sliding mode control applied to a trinary hybrid multilevel inverter. In Proceedings of the 2017 IEEE 3rd Colombian Conference on Automatic Control (CCAC), 2017, pp. 1–6. <https://doi.org/10.1109/CCAC.2017.8276450>.

27. Gray, R.M. *Toeplitz and circulant matrices: a review*; Now Publishers, 2006.

28. Diego Bernal Cobaleda, Miguel Vivert, R.D.G.P. Low-Voltage Cascade Multilevel Inverter with GaN Devices for Energy Storage System. In Proceedings of the 13th IEEE International Conference on Power Electronics and Drive Systems (PEDS 2019), 2019.